Biophysical Chemistry 17 (1983) 139–152
Elsevier Biomedical Press

A SIMPLIFIED APPROACH TO RESONANCE ENERGY TRANSFER IN MEMBRANES, LIPOPROTEINS AND SPATIALLY RESTRICTED SYSTEMS

Michael C. DOODY, Larry A. SKLAR, Henry J. POWNALL, James T. SPARROW, Antonio M. GOTTO, Jr and Louis C. SMITH *

Departments of Medicine and Biochemistry, Baylor College of Medicine and The Methodist Hospital, Houston, TX 77030, U.S.A.

Received 6th May 1982
Accepted 10th November 1982

Key words: Fluorescence; Resonance energy transfer; Membrane; Lipoprotein; Lipid binding

A general model is developed to simulate dipole-dipole resonance energy transfer in spatially restricted systems. At low concentrations of acceptor molecule, the overall quantum yield of a donor population can be defined quantitatively in terms of transfer to multiple defined acceptor regions. Energy transfer at higher acceptor concentrations can be approximated by assuming an exponential dependence of relative quantum yield on the acceptor concentrations. Through geometrical manipulations, this algorithm has been applied using an electronic calculator to systems in which donor-acceptor interaction is limited by unique steric restriction on donor and acceptor distribution within lipid aggregates. The systems that have been analyzed include monomolecular films, bilayer membranes, small discoidal lipid-protein complexes and plasma lipoproteins. The observed energy transfer from *N*-(2-naphthyl)-23,24-*dinor*-5-cholen-22-amide-3β-ol to *N*-dansyldimyristoylphosphatidylethanolamine in a dimyristoylphosphatidylcholine bilayer agrees with that predicted by this model.

1. Introduction

The physical structure of membranes, lipoproteins and lipid-protein complexes has been studied with a wide variety of physical techniques, each with unique limitations and advantages. Förster resonance energy transfer [1] has been used recently to obtain otherwise inaccessible information about the structure of these macromolecular assemblies [2–4]. Recently, several numerical and analytical approaches to energy transfer in two-dimensional structures have been published [2,5–8].

Resonance energy transfer is one of several competitive rate processes involving resonant dipole-dipole interactions between donors and suitable acceptors. For any set of donors and acceptors, the rate constant for energy transfer can be manipulated experimentally. Energy transfer efficiency (T) decreases as the sixth power of the distance (R) separating the two molecules, as described by the following equation.

$$T = (R_0/R)^6/\{1+(R_0/R)^6\} \quad (1)$$

where R_0 is a constant for each donor-acceptor pair and is the distance at which the transfer rate equals the donor decay rate [1]. If the donors and acceptors are randomly distributed, the observed efficiency for transfer from donor to acceptor is a function of acceptor concentration, donor quantum yield, the overlap between donor fluorescence and acceptor absorption spectra, the intermolecular refractive index and a molecular orientation parameter [2].

The complex relationships between structure and chromophore distribution have severely limited quantitative or even qualitative interpretation of energy transfer in many biological systems. In this paper, we present a simplified general method to analyze energy transfer in spatially restricted membrane and lipoprotein systems, with emphasis on the possible structural inferences that can be

* To whom correspondence should be addressed.

0301-4622/83/0000-0000/$03.00

made about these systems. Exclusion of acceptors from the area around the donor, separation of donor and acceptor chromophores, and energy transfer to acceptors distributed in more than one region are important determinants of energy-transfer behavior in biological membranes and in lipoproteins. Energy transfer from the periphery of discoidal systems to the interior is developed here because such structures, containing apoprotein around the circumference, have been postulated for nascent high-density lipoproteins, HDL [9], and some apolipoprotein-lipid complexes [10,11]. Two cases of energy transfer in spherical particles are considered because of the potential use of these techniques in obtaining structural information about the plasma lipoproteins.

2. Experimental procedures

2.1. Materials

3-Acetoxy-*N*-naphthyl-23,24-*dinor*-5-cholen-22-amide [12] was the generous gift of Dr. Yin J. Kao. The acetoxy group was removed by hydrolysis of 400 mg of the compound by refluxing for 30 min with 0.1 M NaOH in methanol. The reaction product was precipitated with H_2O from the cooled solution. The powder was filtered, reprecipitated from CH_3OH/H_2O and recrystallized at $-20°C$ from acetonitrile to yield 340 mg of the crystalline hydroxy derivative. No fluorescent impurities were detected by thin-layer chromatography in hexane/ethyl acetate (7:3, v/v). Natural abundance ^{13}C-NMR confirmed the structure of *N*-naphthyl-23,24-*dinor*-5-cholen-22-amide-3β-ol, NCAd.

Dimyristoylphosphatidylcholine, DMPC (Sigma), was purified on a Waters Model System 500 preparative high-pressure liquid chromatography system equipped with a refractive index detector on a silica column developed isocratically with $CHCl_3/CH_3OH/H_2O$ (60 : 30 : 4, v/v). *N*-Dansyldimyristoylphosphatidylethanolamine (dansyl-DMPE) [13] was the gracious gift of Dr. T.C. Chen and was pure by silica gel thin-layer chromatography in $CHCl_3/CH_3OH/H_2O$ (80 : 20 : 1, v/v).

2.2. Lipid vesicle preparations

Lipids were stored in $CHCl_3$ (Burdick and Jackson, glass distilled) at $-20°C$. Aliquots were evaporated in test tubes under a stream of dry N_2 and dried under high vacuum for 1–2 h, then dissolved in absolute ethanol at 5 mg ml^{-1}.

Vesicles were prepared by injection of an ethanolic solution of phospholipid into buffer with vortex mixing at 37°C [14]. NCAd and dansyl-DMPE, when present, were added to the ethanolic solution in the correct proportions prior to vesicle preparation. Final ethanol concentrations were 2% (v/v).

2.3. Spectroscopic measurements

Fluorescence spectra were collected on an SLM Model 8000 single-photon-counting fluorimeter equipped with a Houston Instruments X-Y recorder and a GCA/McPherson dual-grating excitation monochromator. Corrections were made for photomultiplier tube wavelength response in the calculation of R_0. Temperature was controlled with a Lauda water bath; all solutions were equilibrated with the instrument temperature for 10 min prior to measurement of spectra.

For the calculation of R_0, absorption spectra of dansyl-DMPE were recorded on a Cary Model 15 dual-beam spectrophotometer. A solution of identically prepared but unlabelled vesicles was used as a blank. The absorption spectrum obtained was the same as that published by Vaz et al. [15] for dansylamide in H_2O. R_0 was calculated from the relationship

$$R_0 = [(161.93\kappa^2 JQ)/(\pi^5 n^4 N)]^{1/6} \quad (2)$$

where κ^2 is the orientation parameter, assumed to be 2/3; Q the measured quantum yield; n the refractive index, taken as that of hexane, 1.37; N Avogadro's number and J the spectral overlap integral. The effect of the orientation factor (κ^2) is not considered in the following cases for purposes of simplicity. Thus, R_0 is assumed to be identical for transfer to all acceptor domains. Dale et al. [16] have critically evaluated the importance of the orientation factor and have described a methodology to obtain estimates of the intrinsic uncertainty

in the average value of κ^2 and hence R_0, without restrictive assumptions about the orientations of donors and acceptors in an intramolecular system. J was calculated from the experimental spectra through the relationship

$$J = \int_0^\infty \epsilon(\lambda) F(\lambda) \lambda^4 d\lambda \quad (3)$$

where $\epsilon(\lambda)$ is the molar extinction coefficient of the energy acceptor and $F(\lambda)$ the relative fluorescence intensity of the donor at wavelength λ compared to the total integrated emission spectrum.

2.4. Calculations

All repetitive calculations for each of the models were performed by a Hewlitt-Packard Model 10 programmable desk-top calculator, fitted with Math-pac, printer, and extended RAM memory accessories.

3. Theory

When fluorescent molecules are rigidly and identically coupled in space with chromophore-bearing sites that can accept excited-state energy via dipole-dipole resonance transfer, the resulting donor-acceptor pairs have a characteristic transfer efficiency, T. The relative fluorescence yield, Q_R, of the donor population is equal to $(1 - T)$, where 1 is the fluorescence yield of a population in the absence of the quencher. When only a fraction F of the donor population is coupled to an acceptor molecule in its site, the average relative fluorescence yield of the donor population (Q_{AR}) is greater than that of the completely coupled population. The apparent energy transfer rate constant for transfer to that acceptor site is diminished accordingly. The relative fluorescence yield of the population is an average value, obtained from the equation

$$Q = (1-F)(1) + F(1-T) \quad (4)$$

$$= 1 - FT \quad (5)$$

where F is the fractional occupancy of the acceptor site.

If some individual donors are effectively paired to only one acceptor in one of n possible acceptor sites, Q_R, is

$$Q_R = 1 - \sum_1^n F_i T_i. \quad (6)$$

where F_i is defined as the fractional occupancy of the ith site and T_i the transfer efficiency associated with that site. In actual energy-transfer systems with donors to acceptors randomly distributed within an acceptor domain, the condition that the members of the donor population be effectively linked to either one or no acceptor is met at low acceptor concentration. The acceptor domain is artibrarily divided into 'sites' with different T_i parameters and low acceptor concentrations which yield small F_i values.

These straightforward relationships can be extended by repetitive mechanical calculation to simulate energy transfer in systems of restricted geometry at low acceptor concentration. In the simplest cases, it is possible to construct an acceptor array for each system, which in effect, couples each member of a donor population to multiple acceptor regions with known T and F, so that all points within the effective radius of energy transfer are encompassed.

Since each of the multiple acceptor regions must be given a finite volume or area, transfer efficiency cannot be strictly equal at all points within each. With progressive decreases in the size of the acceptor-containing regions, it can be shown that the function converges. In this study, all calculations, except where noted, are performed with radial increments 1–2 orders of magnitude smaller than strictly necessary. It is also necessary in all calculations to assume a reference concentration of acceptor (C°) that is sufficiently small so that none of the donors interact simultaneously with two or more acceptors. A rigorous solution is obtained at this reference concentration. The dependence of relative fluorescence yield efficiency on acceptor concentration C can be approximated adequately as an exponential function with the following four assumptions, as described by Förster [1]. Energy transfer occurs only from donor to acceptor molecules and the inverse sixth-power dependence holds. Translational motion is slow enough so that each transfer process may be considered at constant distance; whereas molecu-

lar rotation is considered to be much faster than transfer, so that $\kappa^2 = 2/3$ may be used. Förster notes that these conditions are realized approximately in solutions of moderate viscosity.

Values for Q_R at higher experimental concentrations are obtained from the relationship

$$Q_R = Q_R^o(C^o/C) \quad (7)$$

Q_R^o is the relative donor fluorescence yield at the reference acceptor concentration. It is important to bear in mind that neither experimental accuracy nor this exponential relationship holds well when Q_R decreases below 0.2 to 0.3. Energy-transfer experiments should therefore be designed to give more modest reductions in fluorescence yield in order to yield the maximum amount of information.

In some systems every member of the donor population may not be coupled to an identical acceptor matrix. In these cases, it is necessary to divide the donors into subsets in which the distances and orientations of the donor are averaged dynamically, with respect to the acceptor array. The average relative fluorescence yields for each of the subsets can then be calculated. A weighted average relative fluorescence yield for the entire donor population is calculated as follows:

$$Q_{(R)} = (F_{d_1}Q_{R_1}) + (F_{d_2}Q_{R_2}) + (F_{d_3}Q_{R_3}) \ldots + (F_{d_n}Q_{R_n}). \quad (8)$$

The F_d values represent the fraction of the total donor population in each of the n donor regions. The Q_R values are the average relative fluorescence yields of the donors in each region calculated with eqs. 6 and 7. Convergence of the function can also be demonstrated when the sizes of the donor regions are progressively decreased. The averaging procedure greatly extends the applicability of this technique, and may represent the only feasible means of simulating energy-transfer behavior in some systems.

4. Case I – Energy transfer in solution

To test the validity of the method, we have analyzed the case of donors and acceptors in solution, a case previously considered by Förster [1].

The donor is considered to be a single point which is at the center of a sphere which is divided radially into identically incremented shells extending outward a distance of $4R_0$ units. Since energy transfer efficiency decreases with the sixth power of the distance, there is essentially no transfer at greater distances.

To solve the general case, R_0 is set to equal to 1; the acceptor-containing shells are arranged in equally spaced increments, r_a, where r_a is some fraction of R_0; and the acceptor concentration is defined by the number of acceptors/R_0^3.

For the ith shell, the outer radius is equal to $r_a(i)$ and the inner radius is $r_a(i-1)$. The internal volume of the shell is

$$V_i = (4/3)\pi\left[\{r_a(i)\}^3 - \{r_a(i-1)\}^3\right] \quad (9)$$

At low concentrations of acceptor, the fraction of a given shell population that contains one acceptor and therefore the fraction of the donor population with an acceptor in that shell (F_i) is the product of V_i and the acceptor concentration, expressed as the number of acceptors per unit volume. Transfer efficiency is calculated by eq. 1, from the distance from the donor to the midpoint of the shell (an approximation validated by convergence) such that

$$T_i = \left[\{R_0/(r_a(i) - 0.5r_a)\}^6\right] / \left[1 + \{R_0/(r_a(i) - 0.5r_a)\}^6\right] \quad (10)$$

Q_R is then calculated from the F_i and T_i values for each shell in the array with eqs. 6 and 7.

5. Case II – Energy transfer in planar arrays: Membrane and large lipoprotein surfaces

Initial consideration of these systems (fig. 1) is analogous to energy transfer in solution. A single representative donor point is employed, as before. The acceptor matrix, however, is divided into identically incremented concentric circles in a plane, rather than into spherical shells, to a radial distance of $4R_0$. To solve for the general case, R_0 is again assigned a value of 1 and the annuli are incremented as r_a, a fraction of R_0, with acceptor concentration now defined in two-dimensional terms, acceptors/R_0^2 (Fig. 2).

For the specific case of the ith annulus, the outer radius is equal to $r_a(i)$, and the inner radius is equal to $[r_a(i) - r_a]$ or $r_a(i-1)$. The internal area, A_i, of the shell is $\pi[\{r_a(i)\}^2 - r_a(i-1)^2]$. F_i,

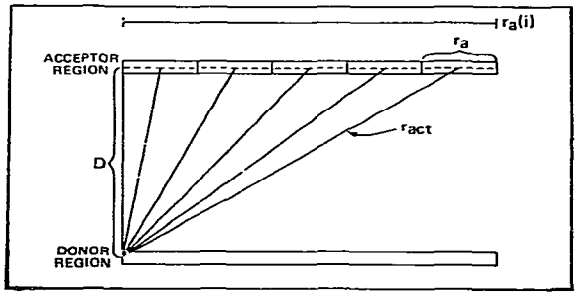

Fig. 1. Energy transfer in planar arrays. D is the average separation of planar donor and acceptor regions; r_a the width of each concentric ring; $r_a(i)$ the outer radius of the ith acceptor region; and r_{act} the distance between each donor and the midpoint of its ith acceptor region.

the fractional occupancy of the concentric region by acceptor chromophores, is equivalent to the product of A_i and the acceptor concentration, now expressed as the number of acceptors per unit area. Transfer efficiency is calculated from the distance from the donor to the midpoint of the shell from eq. 1. As before, the approximation converges to the actual value as r_a is made smaller. The reference donor Q_R is calculated over the

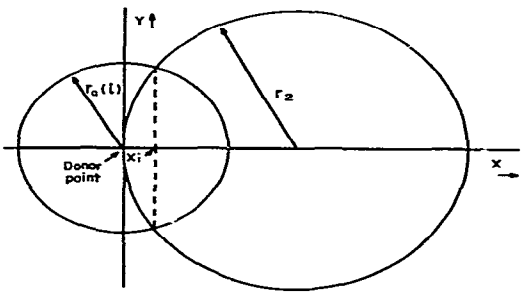

Fig. 2. Energy transfer from the periphery of a planar disc. r_2 is the disk radius and $r_a(i)$ the outer radius of the ith acceptor region. Area of intersection of annulus (i) and the disc is obtained from the sum of the integrals of the r_2 circle area function between donor and x_i, and the $r_a(i)$ circle area function between x_i and $r_a(i)$. This value, minus the area of intersection annulus $r_a(i-1)$, gives the area of the ith shell intersecting the discoidal particle.

acceptor matrix from eq. 6, and the actual donor population Q_R at a given concentration of acceptor is calculated from the relative Q_R by eq. 7.

A special situation occurs when the plane of distribution of the donor array is spatially separated from the plane of distribution of the acceptor array (fig. 1). The method for calculation of F values need not be changed, but the calculation of T values must reflect the increased distance between the donor point and the midpoint of each annulus in the acceptor matrix. The concentric circles in the acceptor matrix are incremented around a reference point in the acceptor plane corresponding perpendicularly to the position of the donor point in the donor matrix. r_{act} is the actual distance in R_0 units between donor and the midpoint of the ith concentric circle and is obtained from the trigonometric equation

$$r_{act} = \left[D^2 + (r_a(i) - 0.5r_a)^2\right]^{1/2} \tag{11}$$

where D is the spatial separation of the donor and acceptor planes in R_0 units.

Calculation of transfer efficiencies for this case requires that the actual distance r_{act} be substituted for R in eq. 1.

$$T = (R_0/R_{act})^6 / \left[1 + (R_0/R_{act})^6\right] \tag{12}$$

Calculation of the donor Q_R proceeds as before.

Donors can also transfer energy simultaneously to the two different spatially separated planar acceptor arrays, when, for example, the donor and acceptor chromophores are situated at fixed depths on different sides of a lipid bilayer. In this case,

$$Q_R = (1 - F_{1A}T_{1A} - F_{1B}T_{1B} - F_{2A}T_{2A} - F_{2B}T_{2B} \cdots - F_{nA}T_{nA} - F_{nB}T_{nB}) \tag{13}$$

where F_A and T_A values are calculated for transfer to the annuli of acceptor plane A, and F_B and T_B values are calculated for transfer to acceptor plane B. Transfer from a single donor plane to multiple acceptor planes can be treated analogously.

It is necessary to recognize that in most real systems the average distance between acceptor chromophores and the donor is restricted sterically. For example, factors such as the presence of a protein around the donor chromophore, the volume of the donor itself and possible electro-

static interactions may have to be considered. These effects may exclude transfer to sites adjacent to the donor in the model. The acceptor matrix may thus be tailored when specific information is assumed or known about the shape or size of the donor. Bilayer curvature is easily taken into account, as necessary, with the methods described in the following sections.

6. Case III – Transfer from donors at the periphery of a disc to acceptors distributed within the disc: Energy transfer in discoidal lipoproteins

This model (fig. 2) is similar to the model for energy transfer in infinite planar arrays, except that a portion of each concentric annulus around the donor point does not intersect the disc and therefore cannot contain acceptors. Geometrical manipulations are therefore needed to account for this fact in the calculation of the F value. All other calculations are performed exactly as for the previous case.

A line is drawn between a donor point at the edge and a point at the center of a disc of radius r_2. This is defined as the x-axis of an x-y coordinate system centered on the donor point and coplanar with the disc. For a given annulus (i) around the donor point (fig. 2), the outer radius $r_a(i)$ intersects the perimeter of the disc at two points corresponding to x_i on the x-axis. At this point, the y values of the circle functions for the outer radius of the annulus and the disc are identical, or

$$y = (r_a(i))^2 - x_i^2 = r_2^2 - (x_i - r_2)^2 \qquad (14)$$

after transformation of the disc coordinates to the center of the x-y coordinate system. This transforms to $x_i = (r_a(i))^2/2r_2$, which permits the calculation of x_i for any given annulus.

The total area $A_{t(i)}$ defined by the intersection of circle $r_a(i)$ with the lipoprotein disc is the sum of the integrals of the disc circle function between the origin and x_i with the integral of the $r_a(i)$ circle function between x_i and $r_a(i)$, or

$$A_{t(i)} = \int_0^{x_i} \left(r_2^2 - (x - r_2)\right)^2 + \int_{x_i}^{r_a(i)} \left[(r_a(i))^2 - x^2\right]^{1/2} \qquad (15)$$

Evaluating between the limits, and summing,

$$\begin{aligned} A_{t(i)} = {} & (\sin^{-1} - 1)(r_a(i))^2 - (\sin^{-1} - 1)(r_2^2) \\ & - \left[\sin^{-1}(r_a(i)/2r_2)\right](r_a(i))^2 \\ & + \left[\sin^{-1}\left(\left[(r_a(i))^2 - 2r_2^2\right]/2r_2^2\right)\right](r_2) \\ & - \left(1 - \left[(r_a(i))^2/4r_2\right]\right)^{1/2}(r_a(i))(r_2) \end{aligned} \qquad (16)$$

The area of the ith annulus that is included in the particle is

$$A_i = A_{t(i)} - A_{t(i-1)} \qquad (17)$$

From this calculated value and the acceptor concentration as the number of acceptors per unit, the F value is calculated as before. The $r_a(i)$ value is incremented to its outer limit of $2r_2$, the diameter of the lipoprotein particle. Calculation of Q_R then proceeds as before. The effects of planar donor-acceptor separation, excluded radius, the ratio of disc diameter to R_0, and presence of a bilayer disc can be considered by the same methods as in the previous model.

7. Case IV – Energy transfer from the surface of a spherical particle to acceptors within its interior and/or in the surrounding medium: Energy transfer in spherical plasma lipoproteins

A three-dimensional coordinate system is defined with the center on a donor point at the surface of a sphere of radius r_2. The x-axis is constructed to intersect the center of the sphere and its surface (fig. 3). The outer radius of the ith spherical shell surrounding the donor point, with a shell radius of $r_a(i)$, intersects the surface of the particle at all points corresponding to x_i on the x-axis. These points define a circle on the surface of the particle. x_i is calculated as before. The sum of the integrals of the volume functions for the lipoprotein particle between the limits of 0 and x_i and the $r_a(i)$ sphere between x_i and $r_a(i)$ gives the included volume of the intersection of the two spheres. The volume of the segment produced by the division of a sphere by a plane is equal to $\left(\frac{\Pi h^2}{3}(3r_2 - h)\right)$, where h is the range of integration and r_2 the sphere radius. This relationship is used to calculate the desired integrals. After trans-

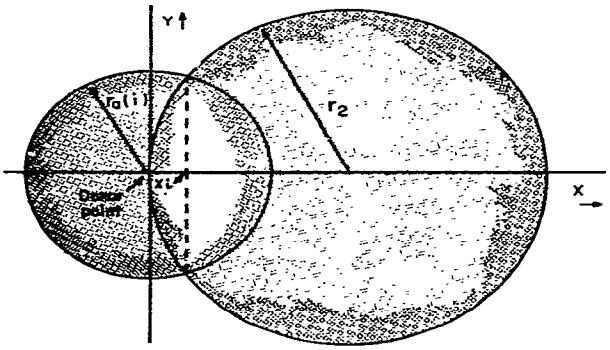

Fig. 3. Energy transfer from donors at the periphery of a lipoprotein to acceptors in the lipoprotein interior. The z-axis is perpendicular to the plane of the drawing. r_2 is the lipoprotein radius. $r_a(i)$ is the outer radius of the ith acceptor region. The volume of intersection of the two spheres is obtained from the sum of the volume integrals for sphere r_2 between the origin and x_i plus that for sphere $r_a(i)$ between x_i and $r_a(i)$. The volume of the intersection of the ith acceptor shell with the lipoprotein is obtained by subtracting the volume of the intersection of shell $(i-1)$ from this sum. Total volume of shell $r_a(i)$ minus its volume intersecting the lipoprotein is the volume of the shell in the exterior medium.

formation of the particle coordinates, the total volume included in the intersection of the two spheres ($V_{t(i)}$) is given as:

$$V_{t(i)} = \left[\frac{\Pi(r_a(i)_2 - x_i)^2}{3}\right]\left[3r_a(i) - (r_a(i) - x_i)\right] + \left[\frac{\Pi(x_i)^2}{3}\right](3r_2 - x_i) \quad (18)$$

The particle volume included within the ith shell ($V_{(i)\text{part}}$) is then calculated as in the previous cases,

$$V_{(i)\text{part}} = (V_{t(i)} - V_{t(i-1)}) \quad (19)$$

In the next steps of the energy transfer calculations, $r_a(i)$ is serially incremented to its outermost limit of $2r_2$, the diameter of the particle. Consideration of some cases of nonrandom acceptor distribution within the particle can be handled by setting different limits on $r_a(i)$ and adopting slightly different procedures for the normalization of particle coordinates.

Calculation of F_i values from the $V_{(i)\text{part}}$ and acceptor concentration and of T_i values from the distances to the midpoint of the shell and then Q_R are done as in the previous case.

The volume of the exterior medium included within the ith shell ($V_{(i)\text{ext}}$) is equal to the total volume of the ith shell minus the volume of the shell intersecting the particle, or

$$V_{(i)\text{ext}} = \left[(4/3)\Pi\left\{r_{(i)}^3 - r_{(i-1)}^3\right\}\right] - V_{(i)\text{part}} \quad (20)$$

For consideration of transfer to the surrounding medium, $r_a(i)$ is incremented to a distance of $4R_0$.

8. Case V – Energy transfer from donors within a spherical particle to acceptors on the particle surface: Energy transfer in plasma lipoproteins

This analysis differs from the preceding cases in one major respect: donors are not all assumed to occupy identical positions with respect to their view of the acceptor matrix. The F_i and T_i values are therefore not the same for the ith shell around every donor. In order to apply the method, it is necessary to analyze separately transfer from unique donor subdomains. These subdomains must be sufficiently small that the view of the acceptor matrix for the donors within each donor region is virtually identical.

Reflection will convince one that the 'appearance' of a featureless sphere is identical from all points within a very thin shell centered upon the same point as the sphere. For this reason the geometry of the donor regions within the sphere will be defined as thin shells. After calculation of Q_R for the donors in each shell, a population average can be calculated as a weighted sum of the average quantum efficiencies from all of its constituent shells (eq. 8).

A donor point is considered in a donor shell of outer radius $s(j)$. A three-dimensional coordinate system is centered on the donor point. This donor shell is within and centered on the same point as the spherical particle or radius r_2 (fig. 4). A concentric acceptor shell, with radius $r_a(i)$, surrounds, and is centered on, the donor point. r_a, r_2 and s are all expressed as small fractions of R_0. In this system, the y value is identical for sphere $r_a(i)$ and sphere r_2 at a point corresponding to x_i on the

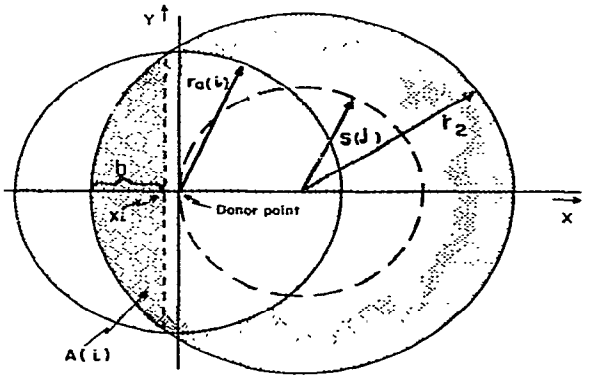

Fig. 4. Energy transfer from donors in the interior of a lipoprotein to acceptors on the lipoprotein surface. r_2 is the lipoprotein radius; $s(j)$ the outer radius of donor shell; $r_a(i)$ the outer radius of the ith acceptor shell; and h the distance from the pole of the lipoprotein to x_i. Point x_i on the x-axis corresponds to the intersection of sphere $r_a(i)$ and the lipoprotein particle. $A_{(i)}$ is the surface area of the lipoprotein from x_i to the pole. $A_{(i)} - A_{(i-1)}$ is the area of intersection of acceptor shell i with the lipoprotein surface. The F value is calculated from this value and the two-dimensional acceptor density. After the relative quantum yields of donors in each donor shell are calculated, a weighted average quantum yield for the total donor population is obtained.

x-axis and 0 on the z-axis. Since the coordinates of the sphere r_2 are displaced in the x-axis by a distance $s(j)$, and for all circles

$$y = (r^2 - x^2)^{1/2} = \left[r_2^2 - (x_i - s(j))^2\right]^{1/2} = \left[\{r_a(i)\}^2 - x_i^2\right]^{1/2}. \quad (21)$$

This relationship simplifies to

$$x_{(i)} = \left[\frac{r_2^2 - (s(j))^2 - (r_a(i))^2}{2s(j)}\right] \quad (22)$$

The nearest pole of the acceptor sphere, when normalized to the coordinates of sphere $r_a(i)$, is at point $\{s(j) - r_a(i)\}$ on the x-axis. The distance h from the pole x_i is therefore calculated as

$$h = x_i - \{s(j) - r_2\} = x_i + r_2 - s(j) \quad (23)$$

The surface area of the r_2 sphere segment from the pole to the circle of intersection with the $r_a(i)$ sphere is the integral of the surface area function of a sphere between $-r_2$ and h, or

$$\text{surface area}_{(i)} = 2\Pi r_2 h \quad (24)$$

The area of the segment on the surface of the spherical particle defined by its intersection with shell $r_a(i)$ is

$$A_n = \text{surface area}_{(i)} - \text{surface area}_{(i-1)} \quad (25)$$

From this area, and the acceptor concentration as the number of acceptors per unit area at the surface of sphere r_2, the F_i and T_i values are calculated as before. Q_R for the donors in donor shell $s(j)$ is calculated from these F and T values for acceptor shells having an $r_a(i)$ betweeen $\{r_2 - s(j)\}$ and $\{r_2 + s(j)\}$. The total volume of the jth donor shell is

$$V_j = (4/3)\Pi\left\{(s_j)^3 - (s_{j-1})^3\right\} \quad (26)$$

For donors randomly distributed within the sphere, the fraction (F_D) of donors within a shell with outer radius $s(j)$ is

$$F_{D_j} = V_{(j)}/\{(4/3)\Pi r_2^3\}. \quad (27)$$

F_{D_j}, of course, must be assigned by different means if donor distribution is assumed not to be random. The weighted relative quantum efficiency (Q_{WR}) of the entire donor population is calculated as the sum of the normalized quantum efficiencies of the donors in each shell.

$$Q_{WR} = \sum_{s(j)=0}^{s(j)=r_2} (F_{D_i})(Q_{R_i}) \quad (28)$$

The final Q_{WR} as a function of acceptor surface density is not a single exponential, as in the previous cases. It is the sum of r_2/s individual exponentials. The function reaches convergence when the increments of s are sufficiently small.

9. Experimental results

The fluorescence excitation and emission spectra of NCAd and dansyl-DMPE in DMPC at 22°C are shown in fig. 5. The overlap between the emission spectrum of NCAd and the absorption spectrum of dansyl-DMPE is quite pronounced, and the spectral overlap integral J calculated by eq. 3 is 3.61×10^{-15}. A quantum yield of NCAd of 0.174 in acetonitrile, which has a polarity equal to that of the bilayer interior at the position of the NCAd chromophore [12], is obtained by compari-

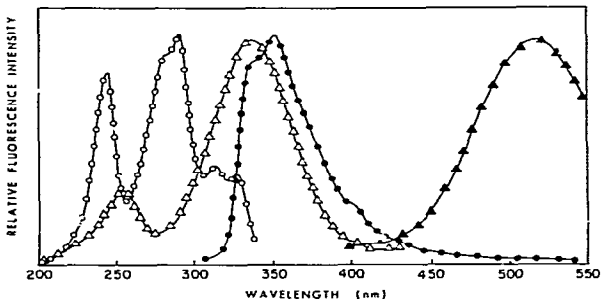

Fig. 5. Spectral overlap of NCAd and dansyl-DMPE. Fluorescence excitation (open symbols) and emission (closed symbols) spectra of NCAd (○,●) and dansyl-DMPE (△,▲) in DMPC vesicles. Probe concentration was 1 mol%; DMPC concentration was 0.29 mM. Temperature was 37°C; slit widths were 0.3 mm for the excitation monochromator and 2 mm for the emission monochromator. The absorption spectrum of dansyl-DMPC has been previously published [15].

son with the integrated spectrum with that of aqueous tryptophan [17] at room temperature. The R_0 for energy transfer from NCAd to dansyl-DMPE is calculated to be 21.6 Å.

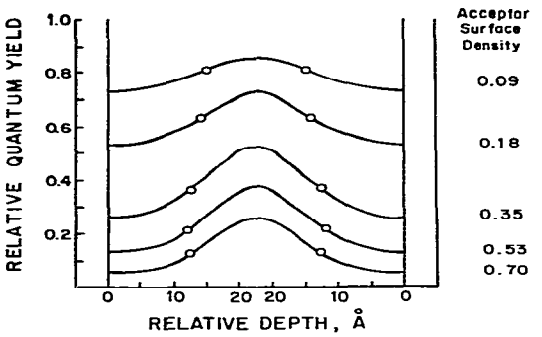

Fig. 6. Determination of depth of NCAd chromophore relative to glycerol backbone region of DMPC. Solid curves are, from top to bottom, the theoretical depth dependence of NCAd quantum yield (eq. 14) at 0.09, 0.18, 0.35, 0.53 and 0.70 acceptors/R_0^2. Bilayer width is assumed to be 45 Å; R_0, 21.6 Å. Excluded radius is assumed to be zero for calculation of theoretical curves. The open circles are the values for relative quantum yield measured at 37°C placed on the theoretical curves for each of the experimental surface densities. The position on the theoretical curve determines the experimentally derived depth. The mean depth obtained by this method is 13.2 ± 1.3 Å.

The measured average relative quantum yields of an NCAd population in DMPC at 37°C containing varying molar concentrations of dansyl-DMPE are shown in fig. 6. The points are placed on theoretical curves generated for a bilayer system. Because the chromophore of dansyl-DMPE is thought to reside at or near the glycerol backbone region [13,15], a planar separation of the two acceptor regions of approx. 45 Å is assumed, based on CPK (Corey-Pauling-Koltun [23]) model building. A liquid-crystalline molecular surface area of 55 Å^2 for saturated phosphatidylcholine is assumed, based upon monolayer force-area data [18]. No excluded radius is assumed for these calculations. Conversion from mole fraction dansyl-DMPE in DMPC to acceptor concentrations in terms of R_0^2 is made from the relationship

$$\text{acceptor concentration} = (R_0^2)(\text{mol fraction dansyl-DMPE})/55\ \text{Å}^2 \quad (29)$$

Averaging of the data indicates that the naphthyl group is 13.2 ± 1.3 Å from the level of dansyl-DMPE. CPK molecular models, with placement of the 3-hydroxy function of NCAd at the ester carbonyl region, predict a distance of 14–17 Å. This comparison indicates reasonable agreement between the data and the model.

10. Discussion

Energy transfer to acceptors randomly distributed in a three-dimensional array has been analyzed by this algorithm in order to compare the results with those obtained previously. Diffusion of acceptors in the lifetime of the donor excited state is not considered, since diffusion is not significant on the nanosecond time scale in systems with viscosities comparable to those in lipid domains. Q_R values determined by this method after convergence and by numerical solution of Förster's formalism [19,20] are compared in fig. 7 for ideal solutions as a function of acceptor concentration. The agreement clearly validates the present method and suggests that it can be extended profitably to other systems.

The same algorithm can be extended to energy transfer in two-dimensional systems. Since this

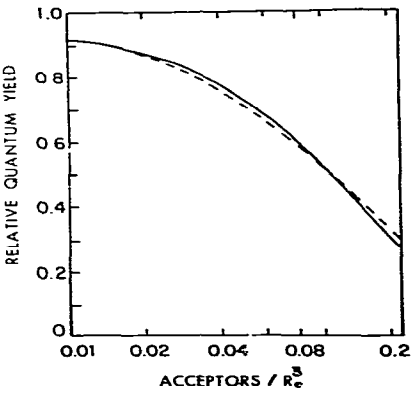

Fig. 7. Energy transfer in three-dimensional solutions. Relative quantum yield vs. acceptor concentration determined by numerical solution of the Förster equations (— — —) and by concentric acceptor region algorithm (———).

system has also been considered by other workers, it is possible to compare these results with those that are obtainable by two analytical approaches. Fig. 8 shows excellent agreement between the three methods over the entire range of experimentally useful quantum yields. Spatial restrictions on donor-acceptor approach can be taken into account. The general solution for monolayers at several acceptor densities is presented in fig. 9. It

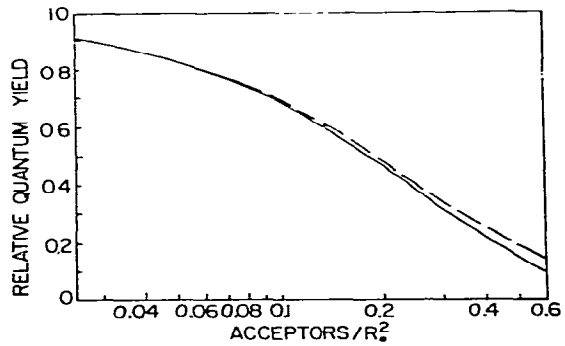

Fig. 8. Energy transfer in planar systems. Relative quantum yield vs. acceptor concentration determined by analytical methods [5,8] (— — —) and by concentric acceptor region algorithm (———).

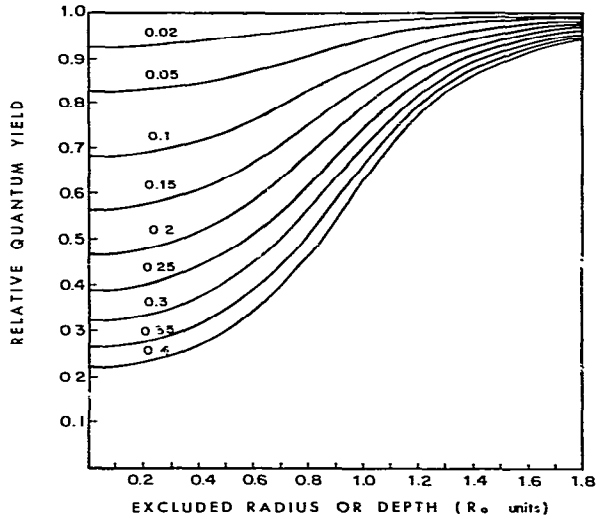

Fig. 9. Effect of horizontal or vertical separation of donor and acceptor on transfer efficiency in planar arrays. Acceptor concentrations (0.02–0.4) are given as the quantity (number of acceptors)/R_0^2. Excluded radius (horizontal separation) and depth (vertical separation) have identical effects on transfer efficiency.

is of interest to note that for geometrical reasons, when excluded radius is put in terms of R_0, the overall transfer efficiency is affected in the same way as by changes in D, the spatial separation of the donor and acceptor planar arrays. A given experimentally determined quantum yield at fixed acceptor concentration can thus be the result of a combination of effects due to plane separation and excluded radius. Results of a program designed to illustrate the nature of this relationship are shown in fig. 10.

For this calculation, the acceptor concentration is held at 0.5 acceptors/R_0^2. The combination of depth and excluded radius, which can give rise to any given experimentally measured relative quantum yield, defines a circle on an x-y plot of the two parameters, and no information is made available on the actual importance of either factor.

Despite this limitation, it should be possible in some cases to determine exact values for the excluded radius and spatial separation of the donor

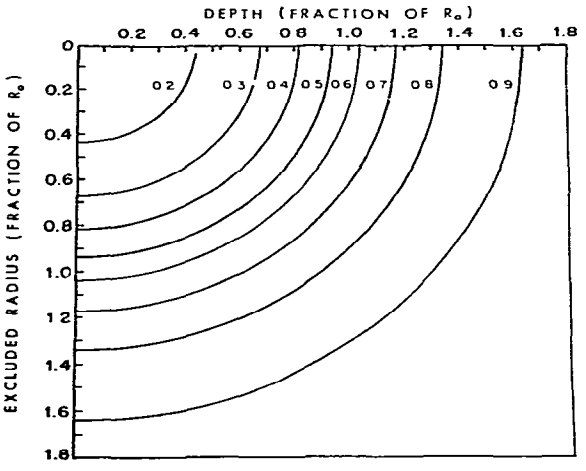

Fig. 10. Effect of horizontal and vertical separation in combination on transfer efficiency in planar arrays. Depth and excluded radius are both expressed in terms of R_0. Actual acceptor density is $0.5/R_0^2$. The calculated lines represent the possible depth/excluded radius relationships for donors with the indicated relative quantum yields, which range from 0.2 to 0.9 in this figure.

and acceptor plane through comparison of these transfer results with the results seen for transfer to an other molecular species of acceptor, whose distribution is confined to another plane. This requires prior determination of the spatial separation of the planes of two kinds of acceptor by these or other techniques.

It must also be remembered that the acceptors confined to each of the two leaflets of a bilayer do not necessarily have identical distributions. For example, a fluorescently labeled protein on one side of a bilayer membrane may exclude acceptors from a significant area on its side, but none on the other.

Although an excluded radius allows for the representation of steric effects, the real situation may not be represented adequately. In cases where some information is available, it is profitable to tailor the acceptor matrix to the nature of the exclusion properties of the system. One example of this would be the transfer of energy from the tryptophan of lipid-binding proteins to chromophore-containing lipids. Many proteins are thought to bind lipid as amphipathic helices [21]. It is a reasonable approach to construct an acceptor matrix for these systems which places the tryptophan at the center of a 10 Å ribbon into which acceptor cannot penetrate; the areas of each of the n acceptor regions can then be adjusted for the excluded areas by simple geometric manipulations. More directly, space-filling models can be built of the appropriate peptide region and projected onto graph paper in a theoretically acceptable orientation, with the boundary of the hydrophilic and hydrophobic faces parallel to the plane of the paper. This procedure is illustrated as an example in fig. 11 for LAP-20, a synthetic lipid-associating peptide [22] that binds phosphatidylcholine, presumably as an α-helix. The excluded areas are then determined by manual techniques such as square counting. A modified program is required to handle these calculations. This program reduces the F_i values in proportion to the ratio of excluded area to total area of each radial acceptor subdomain. Interestingly, the calculated donor quantum yield parameters for tryptophan at the center of the LAP-20 peptide are essentially identical when calculated by the 10 Å ribbon and graphic techniques. This approach may be useful in determining the depth of the tryptophan residues of lipid-binding peptides.

Energy transfer in monolayer discs is considered in Case III, and the results are easily extended to bilayer disc models. It is of interest to note that in the monolayer disc model the effect of excluded radius and donor/acceptor planar separation are not identical, as they are in the monolayer plane model; the relative magnitude of this discrepancy is a function of the ratio of the particle radius to R_0 (not shown). The effect of r_2/R_0 ratio on transfer efficiency at a fixed acceptor concentration is shown in fig. 12. At very low r_2/R_0 ratios, the size of the disc is insignificant with respect to the effective domain of energy transfer, and little or no transfer efficiency occurs. On the other hand, as the r_2/R_0 ratio is increased, the transfer efficiency tends toward a constant value, which is the square root of the Q_R seen in an infinite planar array at the same surface density.

This relationship is clarified if one considers a line passing through the donor point, dividing the plane into A and B halves. It is clear that the

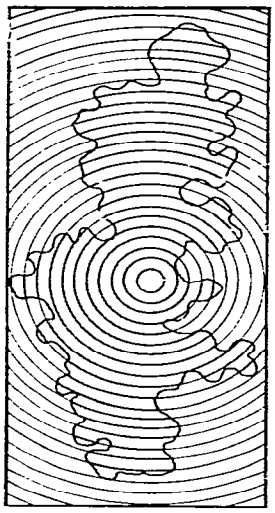

Fig. 11. Exclusion of acceptor from approach to the tryptophan of lipid-associating peptide 20. CPK models of the peptide are constructed in an α-helical configuration. The boundary of the hydrophobic and hydrophilic faces is approximately parallel to the surface. An outline of the peptide is projected onto a matrix of 1 Å concentric acceptor regions surrounding the tryptophan residue of the peptide. Transfer efficiencies, calculated from regions of this size, typically are within 1–3% of their limiting values at convergence, depending on the magnitude of R_0 and the acceptor concentrations. The amino acid sequence of LAP-20 is NH_2-Val-Ser-Ser-Leu-Leu-Ser-Ser-Leu-Lys-Glu-Tyr-Trp-Ser-Ser-Leu-Lys-Glu-Ser-Phe-Ser-COOH [22]. The amino terminal of the peptide is at the top of the figure.

donor Q_R due to transfer to either side alone is equal to that due to transfer to the other side, or $Q_{R(A)} = Q_{R(B)}$. In addition, the overall Q_R is the product of the relative quantum efficiencies due to transfer to both sides. Since the acceptor dependence of quantum yield is assumed to be exponential, then

$$Q_R = Q_{R(A)} Q_{R(B)} = (Q_{R(B)})^2 \tag{30}$$

and therefore

$$Q_{R(B)} = Q_R \tag{31}$$

At high r_2/R_0 ratios, the situation tends toward

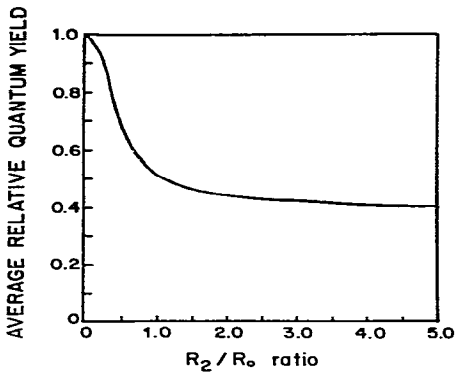

Fig. 12. Effect of particle dimensions on energy transfer from the periphery of a planar disc. Relative donor quantum yield ranges from essentially unity at low r_2/R_0 ratios to a constant value at high r_2/R_0 ratios.

the case of transfer to one side of a divided plane as the curvature of the disc becomes small relative to the effective domain of energy transfer. This analysis is included because of the current interest in the structure of small apolipoprotein complexes and newly secreted 'nascent' HDL. Energy-transfer experiments have the potential to resolve the spatial arrangement of the protein and lipid in these particles.

Energy transfer from donors on the surface of a sphere to acceptors within the lipoprotein interior or on the lipoprotein exterior is examined in Case IV. Fig. 13 gives the theoretical dependence of donor population quantum efficiency on the ratio of the particle radius to R_0 at a fixed acceptor concentration.

For transfer to the exterior of the particle, values of energy transfer are seen at low ratios which tend toward the value representative of transfer in solution as the size of the particle becomes insignificant with respect to the effective domain of energy transfer. At high ratios, the quantum efficiency value tends toward a value which is the square root of solution Q_R, as would be expected if all acceptors were confined to one side of a plane containing the donor molecules.

For the case of acceptors in the interior of the particle, little or no energy transfer is seen at low

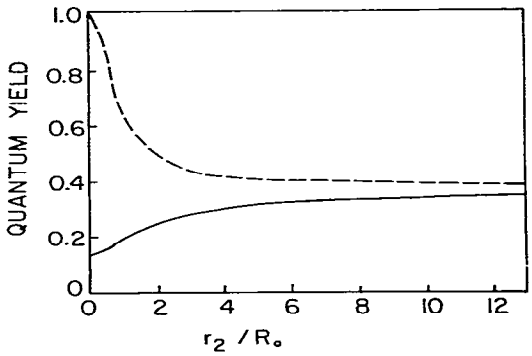

Fig. 13. Effect of lipoprotein dimensions on energy transfer from donors at its surface. Acceptor concentration is $0.3/R_0^3$ in the lipoprotein interior (— — —) or exterior (———). In both cases, the quantum yield of the donor tends toward a constant value at high r_2/R_0 ratios. Energy-transfer efficiency to acceptor in the interior tends toward zero at low r_2/R_0 ratios, while transfer efficiency to acceptors in the exterior tends toward the value for unrestricted solutions.

ratios, because the size of the acceptor-containing particle is not significant. At high ratios, the quantum efficiency again approaches the square root of the quantum efficiency due to energy transfer in solution, for the same reason as before.

When donor transfers energy to some acceptor capable of partitioning into both the interior and exterior domains,

$$Q_R = 1 - T_{\text{interior}} - T_{\text{exterior}} \quad (32)$$

The interior and exterior parameters reflect differences in acceptor concentration and R_0 in the two environments. Transfer experiments to the medium surrounding the particle must be made under conditions of high external viscosity in order to minimize the effect of diffusion during the donor fluorescence lifetime.

The localization of the chromophore of NCAd, a fluorescent cholesterol analogue, has been determined in relation to the dansyl-DMPE chromophore in DMPC bilayer membranes by analysis of energy-transfer data. The localization is in good agreement with what is expected based upon the previous determination of the dansyl-DMPE head group position and the length of the sterol probe as determined by CPK model building. This finding reinforces the conclusion that the polarity-sensitive *N*-(2-naphthyl)-23,24-*dinor*-5-cholen-22-amine-3β-ol [12] is a probe of the bilayer interior.

It has been shown that energy transfer in systems modeled after biologically important lipid entities is sensitive to the structural features of the models. When valid assumptions can be made about some of these structural features or probe location, energy transfer can be useful in describing other features in qualitative and/or quantitative terms. These features include particle geometry and dimensions, location of donor and acceptor domains in relation to one another, probe distribution with domains and steric restrictions on the mutual approach of donor and acceptor chromophores.

Acknowledgements

This work was supported by The Robert A. Welch Foundation Grants Q-343 and Q-90€; the National Heart and Blood Vessel Research and Demonstration Center, Baylor College of Medicine, a grant supported research project of the National Heart, Lung and Blood Institute HL-17269; HHS Grants HL-15648 and HL-19459. L.A.S. was a Helen Hay Whitney Postdoctoral Fellow and is now at the Scripps Clinic and Research Foundation, La Jolla, CA. M.C.D. was a Robert A. Welch Predoctoral Fellow.

References

1 T. Förster, Disc. Faraday Soc. 27 (1959) 7.
2 B. Fung and L. Stryer, Biochemistry 17 (1978) 5241.
3 J.M. Vanderkooi, A. Ierokomas, H. Nakamura and A. Martonosi, Biochemistry 16 (1977) 1262.
4 L.A. Sklar, M.C. Doody, A.M. Gotto, Jr and H.J. Pownall, Biochemistry 19 (1980) 1294.
5 T.G. Dewey and G.G. Hammes, Biophys. J. 32 (1980) 1023.
6 T.N. Estep and T.E. Thompson, Biophys. J. 26 (1979) 195.
7 D.E. Koppel, P.J. Fleming and P. Strittmatter, Biochemistry 18 (1979) 5450.
8 P.K. Wolber and B.S. Hudson, Biophys. J. 28 (1979) 197.
9 R.L. Hamilton, M.C. Williams, C.J. Fielding and R.J. Havel, J. Clin. Invest. 58 (1976) 667.
10 A.R. Tall, D.M. Small, R.J. Deckelbaum and G.G. Shipley, J. Biol. Chem. 252 (1977) 4701.

11 J.P. Segrest, Chem. Phys. Lipids 18 (1977) 7.
12 Y.J. Kao, A.K. Soutar, K.H. Hong, H.J. Pownall and L.C. Smith, Biochemistry 17 (1978) 2689.
13 A.S. Waggoner and L. Stryer, Proc. Natl. Acad. Sci. U.S.A. 67 (1970) 579.
14 S. Batzri and E.D. Korn, Biochim. Biophys. Acta 298 (1973) 1015.
15 W.L.C. Vaz, K. Kaufman and A. Nicksch, Anal. Biochem. 83 (1977) 385.
16 R.E. Dale, J. Eisinger and W.E. Blumberg, Biophys. J. 26 (1979) 161.
17 F.W.J. Teale and G. Weber, Biochem. J. 65 (1957) 476.
18 S.W. Hui, M. Cowden, D. Paphadjopoulos and D.F. Parsons, Biochim. Biophys. Acta 382 (1975) 265.
19 J. Feitelson, J. Chem. Phys. 44 (1966) 1497.
20 Y. Elkana, J. Feitelson and E. Katchalski, J. Chem. Phys. 48 (1968) 2399.
21 J.P. Segrest, R.L. Jackson, J.D. Morrisett and A.M. Gotto, Jr. FEBS Lett. 38 (1974) 147.
22 J.T. Sparrow and A.M. Gotto, Jr, Ann. N.Y. Acad. Sci. 348 (1980) 187.
23 W.L. Koltun, Biopolymers 3 (1965) 665.